Supplementary Information

Synergistic Self-Assembly and High-Entropy Dual Engineering of the Ruddlesden-Popper Air Electrode Enable High-performance and Stable Reversible Protonic Ceramic Cells

Qiang Xue [a], Guangjun Zhang [a], Ting Chen [*a], Guozhu Zheng [a], Chenxiao Wang [a], Zichen Zhuang [a], Kui Liu [a], Yucun Zhou [*b], Lang Xu [a], Shaorong Wang [*a]

a School of Chemical Engineering&Technology, China University of Mining and Technology, 1 Daxue Street, Xuzhou, Jiangsu Province, 221116, China

b Beijing Huairou Laboratory, Beijing, 101400, China

* Corresponding authors.

E-mail addresses: chenting@cumt.edu.cn (T. Chen), srwang@cumt.edu.cn (S. Wang), zhouyucun@hrl.ac.cn (Y. Zhou)

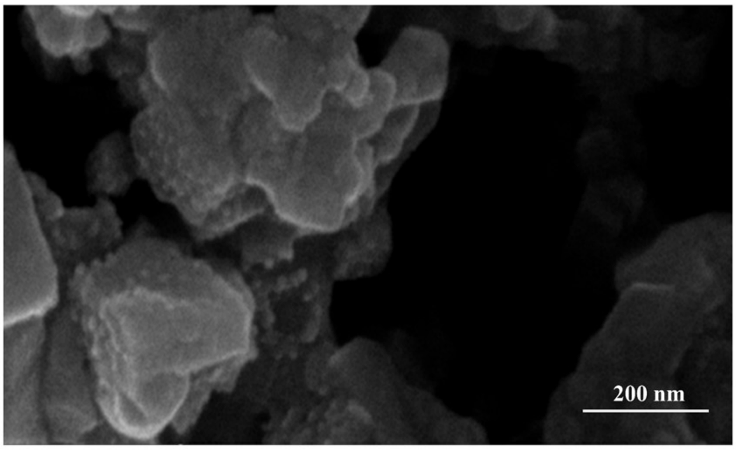

Fig. S1. SEM image of the as-synthesized PSNLGCN powder fired at 1000 °C for 3 h.

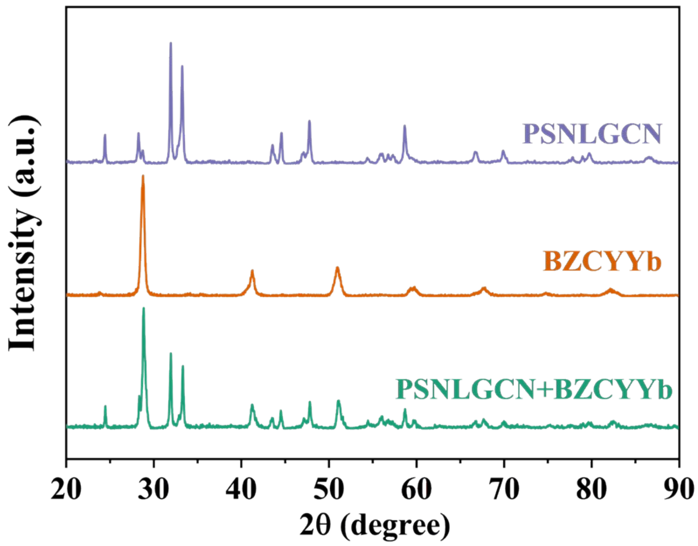

Fig. S2. XRD patterns of PSNLGCN, BZCYYb, and their mixture (mass ratio of 1:1) powders after being fired at 1050 °C for 5 h in air.

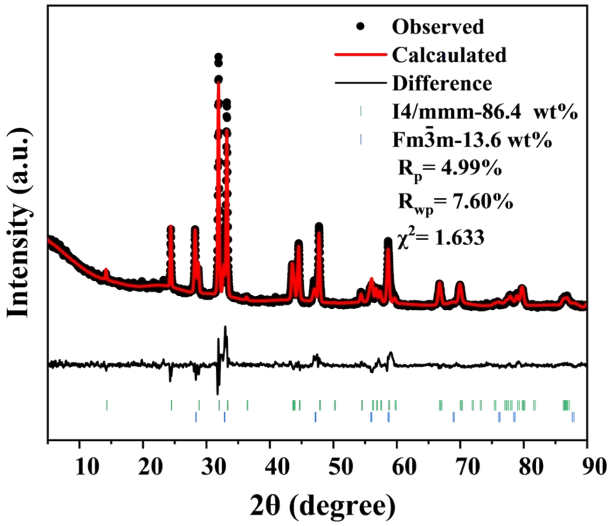

Fig. S3. XRD refinement of PSNLGCN after the treatment in 30% H_2O-air at 650 °C for 100 h.

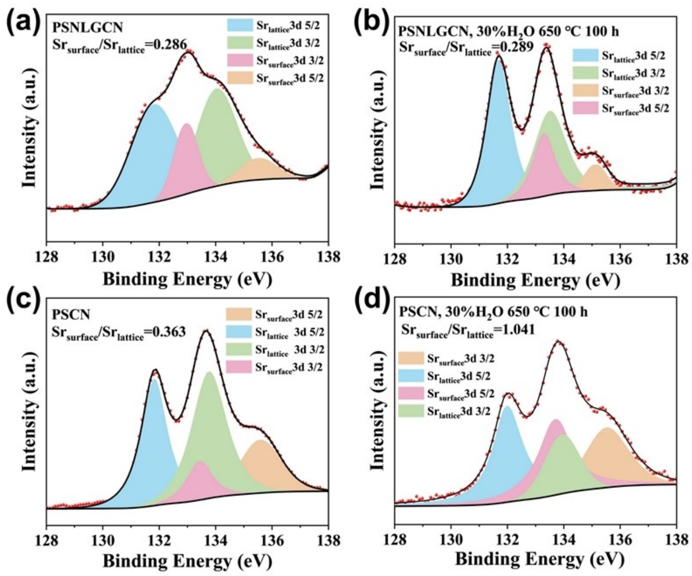

Fig. S4. Comparison of Sr 3d XPS profiles of (a-b) PSNLGCN and (c-d) PSCN powders before and after the treatment in 30% H_2O-air at 650 °C for 100 h.

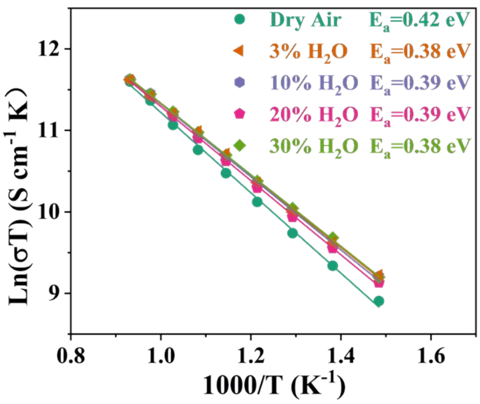

Fig. S5. The Arrhenius plots of the conductivities of PSNLGCN in air with 0-30% H_2O.

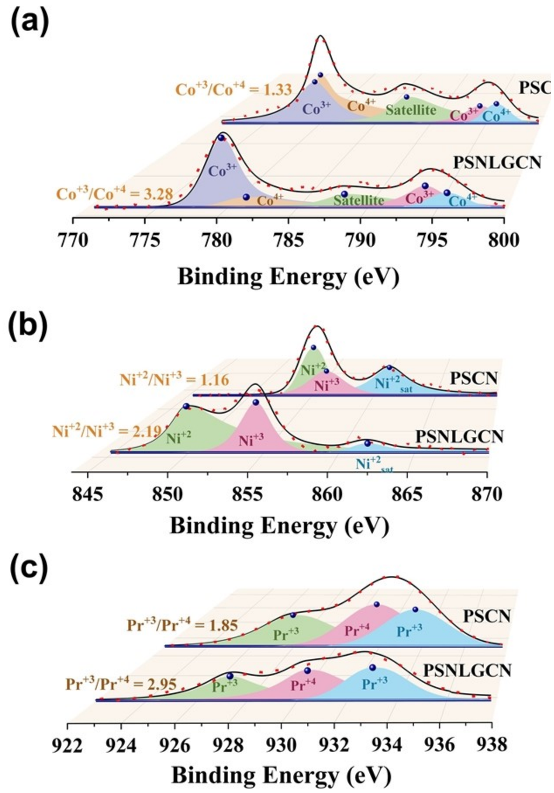

Fig. S6. (a) Co 2p XPS spectra of PSNLGCN and PSCN; (b) Ni 2p XPS spectra of PSNLGCN and PSCN; (c) Pr 3d XPS spectra of PSNLGCN and PSCN.

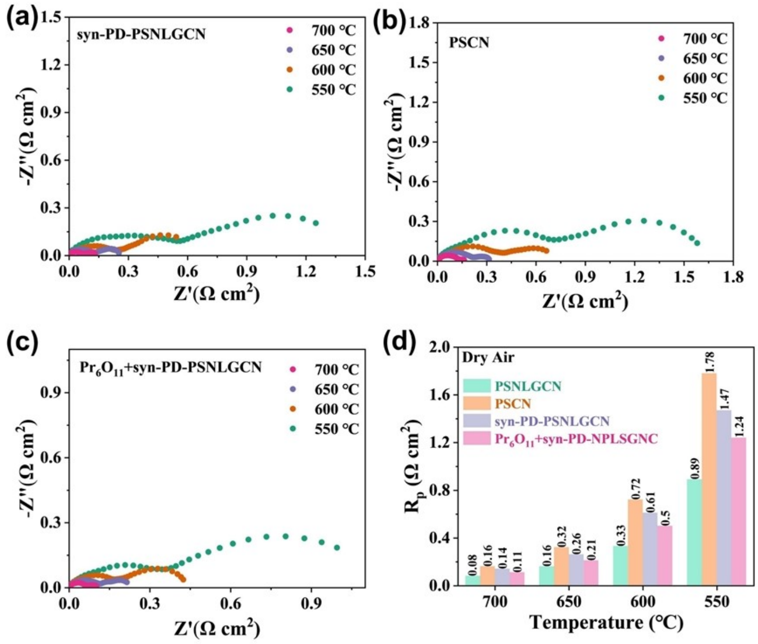

Fig. S7. EIS of symmetric cells with syn-PSNLGCN, PSCN, and Pr_6O_{11}+syn-PD-PSNLGCN air electrodes. (a) syn-PD-PSNLGCN, (b) PSCN, and (c) Pr_6O_{11}+syn-PSNLGCN in dry air; (d) the corresponding R_p values.

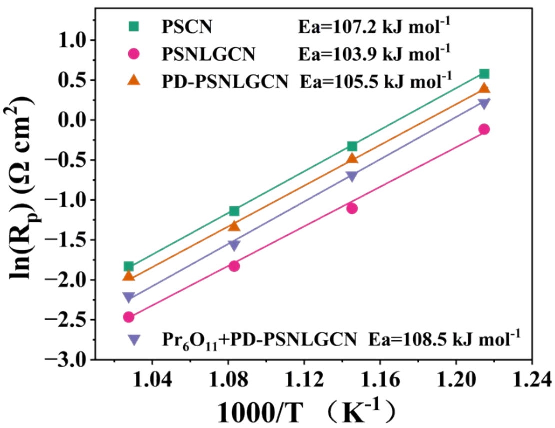

Fig. S8. Temperature dependence of the R_p of PSCN, PSNLGCN, PD-PSNLGCN and Pr_6O_{11}+PD-PSNLGCN air electrodes.

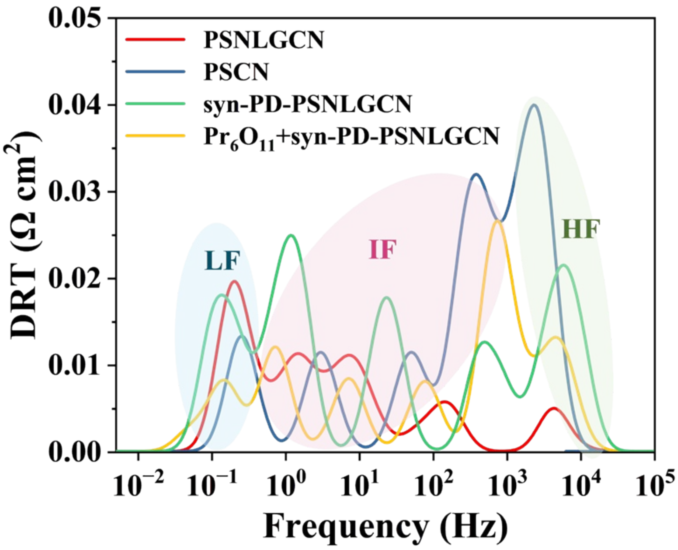

Fig. S9. DRT analysis of PSNLGCN, PSCN, syn-PD-PSNLGCN, and Pr_6O_{11}+syn-PD-PSNLGCN in dry air at 700 °C.

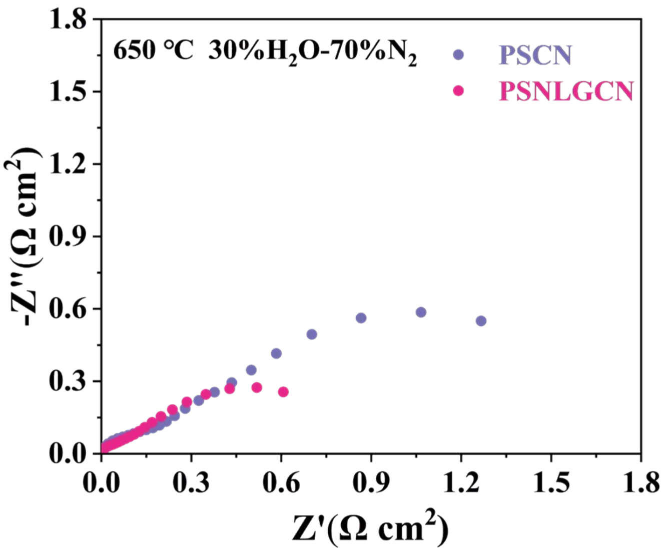

Fig. S10. EIS plots of PSNLGCN and PSCN at 650 °C in 30% H_2O-70% N_2.

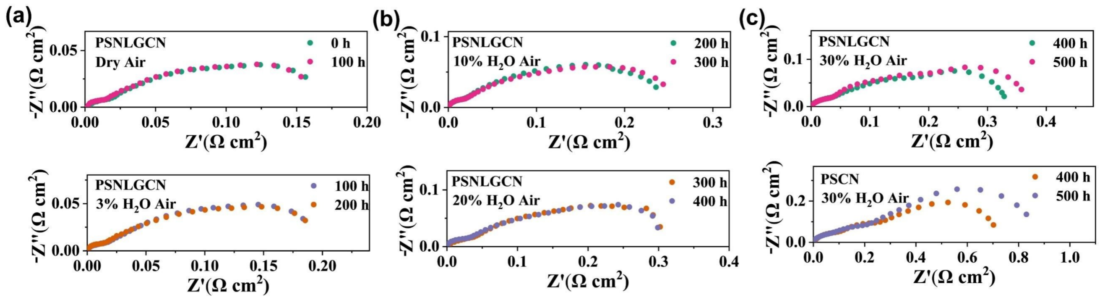

Fig. S11. EIS curves of PSNLGCN air electrode at 650 °C (a) at 0 h and 100 h in dry air, and at 100 h and 200 h in 3% H_2O air; (b) at 200 h and 300 h in 10% H_2O air, and at 300 h and 400 h in 20% H_2O air; (c) EIS curves of PSNLGCN and PSCN air electrodes at 650 °C at 400 h and 500 h in 30% H_2O air.

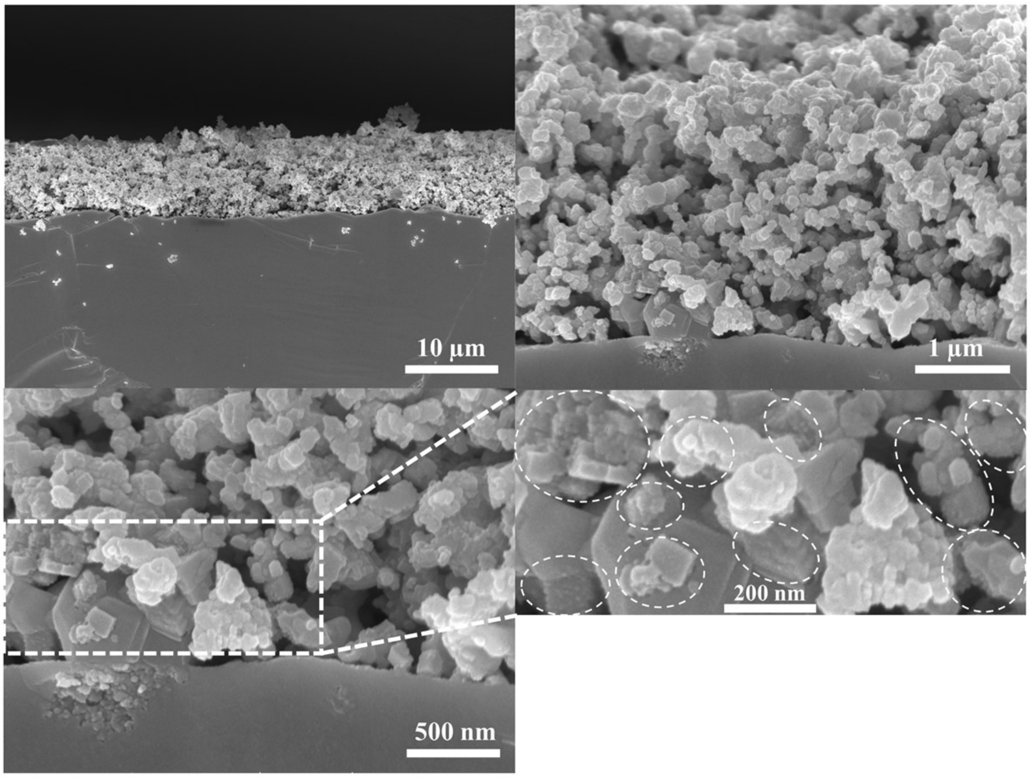

Fig. S12. The microstructure of the symmetrical cell with PSNLGCN composite electrode after 500 h long-term test under varying steam pressures.

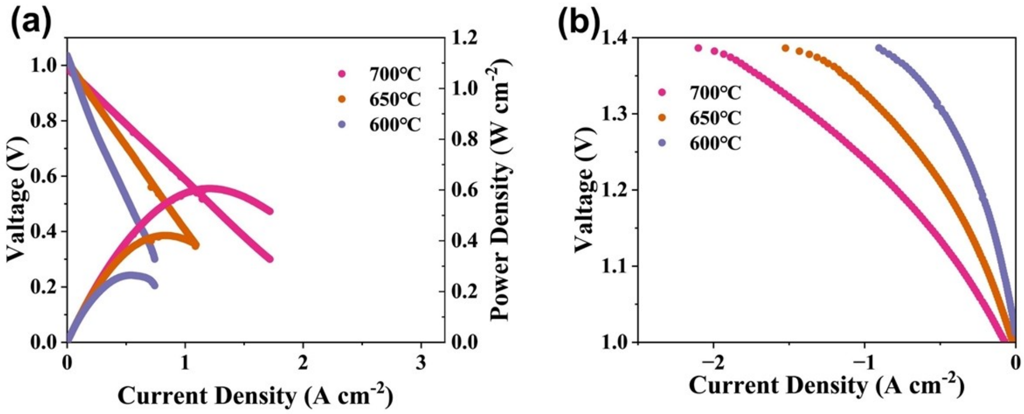

Fig. S13. Electrochemical performance of RPCC with the PSCN air electrode. (a) I-V-P curves of the cell measured in FC mode at 600-700 ℃; (b) The I-V curves of the cell in EC mode at 600-700 ℃.

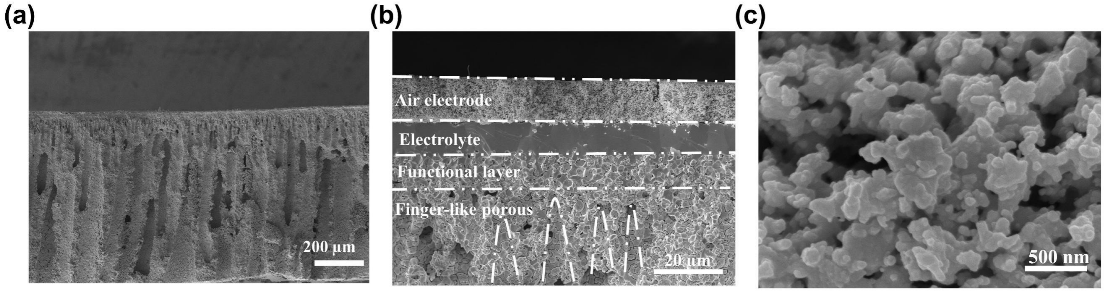

Fig. S14. Cross sectional SEM images of the cell with the PSNLGCN air electrode after the stability testing. (a) Overall view; (b) Air electrode-electrolyte-fuel electrode; (c) Air electrode.

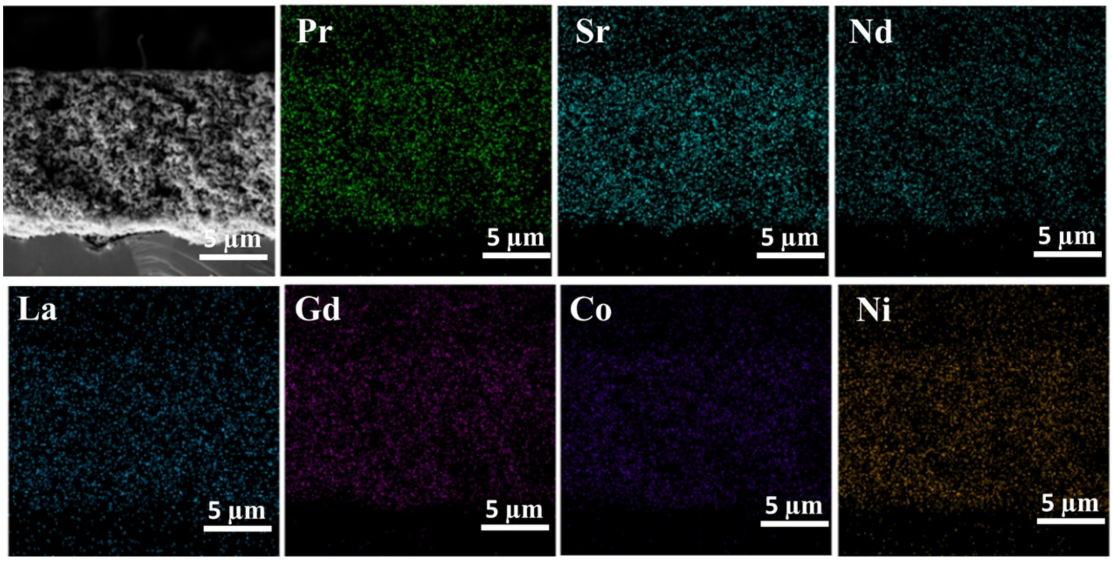

Fig. S15. The EDS elemental mapping of the PSNLGCN air electrode after the stability test.

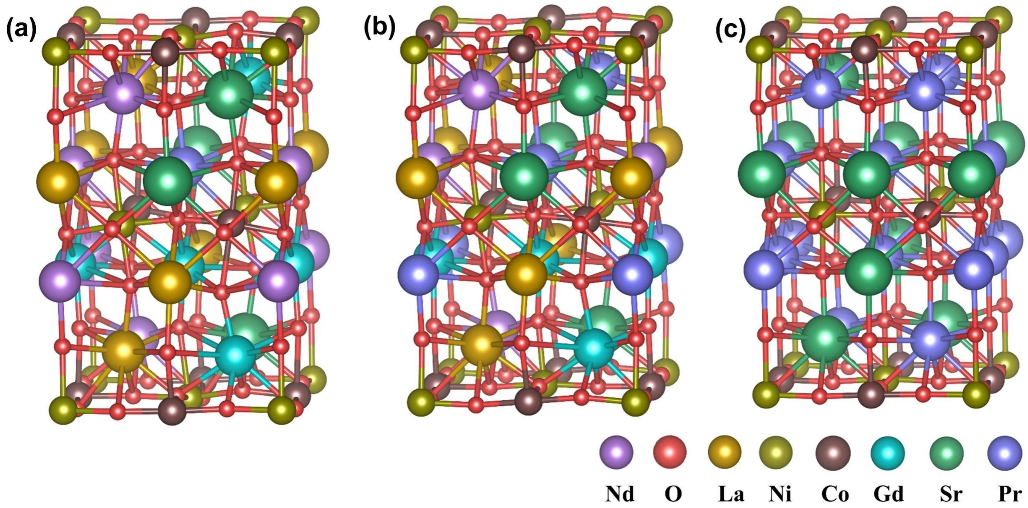

Fig. S16. DFT calculation model for (a) PD-PSNLGCN; (b) perfect configuration PSNLGCN; (c)PSCN.

Table S1. Refinement parameters of PSNLGCN oxide calcinated at 950 °C for 5 h in air.

Element	Label	x	y	z	Occupancy
Phase 1 (PD-PSNLGCN, I4/mmm, a=b=3.798 Å c=12.369 Å, 87.1 wt%)					
Nd	Nd1	0	0	0.361185	0.237
Pr	Pr1	0	0	0.361185	0.0525
La	La1	0	0	0.361185	0.237
Sr	Sr1	0	0	0.361185	0.237
Gd	Gd1	0	0	0.361185	0.237
Ni	Ni1	0	0	0	0.5
Co	Co1	0	0	0	0.5
O	O1	0	0.5	0	1
O	O2	0	0	0.163916	1
Phase 2 (Pr_6O_{11}, Fm-3m, a=b=c=5.4482 Å, 12.9 wt%)					
Pr	Pr1	0	0	0	1
O	O1	0.25	0.25	0.25	0.995

Table S2. The atomic ratio of each element in as-synthesized PSNLGCN, measured by inductively coupled plasma optical emission spectroscopy (ICP-OES).

Sample	Pr	Sr	Nd	La	Gd	Co	Ni
PSNLGCN	0.401	0.399	0.400	0.401	0.400	0.499	0.500

Table S3. Refinement parameters of PSNLGCN powder at 650 °C for 100 h in wet air (30% H_2O).

Composition	R_p (%)	R_{wp} (%)	χ^2	Space group	a (Å)	b (Å)	c (Å)	Occupancy (wt%)
PD-PSNLGCN	4.99	7.60	1.633	I4/mmm	3.796	3.796	12.361	86.4
Pr_6O_{11}	4.99	7.60	1.633	Fm-3m	5.449	5.449	5.449	13.6

Table S4. The R_p of symmetrical cells with PSNLGCN and other high-performance RP-type electrodes reported recently.

Air electrode	Electrolyte	Temperature (°C)	R_p (Ω cm^2)	Reference
$La_3Ni_2O_{7-\delta}$ (LNO)	BZCY	700	0.089	1
		650	0.25	
		600	0.83	
		550	2.1	
$Sr_3Fe_{1.5}Zn_{0.5}O_{7-\delta}$ (SFZ)	BZCY	700	0.15	2
		650	0.47	
		600	1.3	
$Sr_3Fe_{1.3}Co_{0.2}Mo_{0.5}O_{7-\delta}$-$BaZr_{0.1}Ce_{0.7}Y_{0.2}O_{3-\delta}$ (SFCMO-BZCY)	BZCY	700	0.96	3
		650	1.56	
		600	3.1	
$Pr_{1.2}Sr_{0.8}NiO_{4+\delta}$ (PSN)	BZCY	700	0.14	4
		650	0.29	
		600	0.58	
		550	1.35	
$LaSr_{2.7}Co_{1.5}Fe_{1.5}O_{10-\delta}$ (LSCF2.7)	BZCYYb	700	0.09	5
		650	0.2	
		600	0.44	
		550	1.2	
$Pr_{0.4}Sr_{0.4}Nd_{0.4}La_{0.4}Gd_{0.4}Co_{0.5}Ni_{0.5}O_{4+\delta}$ (PSNLGCN)	**BZCYYb**	**700**	**0.08**	**This work**
		650	**0.16**	
		600	**0.33**	
		550	**0.89**	
$Pr_{1.2}Sr_{0.8}Co_{0.5}Ni_{0.5}O_{4+\delta}$ (PSCN)	**BZCYYb**	**700**	**0.16**	**This work**
		650	**0.32**	
		600	**0.72**	
		550	**1.78**	

BZCY: $BaCe_{0.7}Zr_{0.1}Y_{0.2}O_{3-\delta}$
BZCYYb: $BaZr_{0.1}Ce_{0.7}Y_{0.1}Yb_{0.1}O_{3-\delta}$

Table S5. Performance (FC mode) comparison of the PSNLGCN with others RP-type air electrode previously reported.

Air electrode	Electrolyte thickness (μm)	Temperature (°C)	PDD (W cm^{-2})	Reference
$La_{0.6}Sr_{0.4}FeO_{3-\delta}$-$La_{1.2}Sr_{0.8}NiO_{4+\delta}$ (LSF-LSN)	70	700	0.34	6
		650	0.24	
		600	0.18	
		550	0.1	
$Sr_3Fe_{1.3}Co_{0.2}Mo_{0.5}O_{7-\delta}$-$BaZr_{0.1}Ce_{0.7}Y_{0.2}O_{3-\delta}$ (SFCMO-BZCY)	20	700	0.39	3
		650	0.29	
		600	0.19	
$La_{1.2}Sr_{0.8}NiO_{4+\delta}$ (LSN)	15	700	0.46	7
		650	0.33	
		600	0.22	
$Sr_3Fe_{1.5}Zn_{0.5}O_{7-\delta}$ (SFZ)	100	700	0.46	2
		650	0.31	
		600	0.15	
$LaSr_{2.7}Co_{1.5}Fe_{1.5}O_{10-\delta}$ (LSCF2.7)	28	700	0.56	5
		650	0.52	
		600	0.39	
		550	0.24	
$La_{1.6}Sr_{0.4}Cu_{0.6}Ni_{0.4}O_{4+\delta}$ (LSCN)	10	700	0.73	8
		650	0.5	
		600	0.27	
$La_3Ni_{1.6}Co_{0.4}O_{7-\delta}$ (LNCO)	/	700	0.398	9
		650	0.293	
		600	0.215	
$Pr_{0.4}Sr_{0.4}Nd_{0.4}La_{0.4}Gd_{0.4}Co_{0.5}Ni_{0.5}O_{4+\delta}$ (PSNLGCN)	**10**	**700**	**1.1**	**This work**
		650	**0.71**	
		600	**0.39**	
		550	**0.18**	

Table S6. Performance (EC mode) comparison of the PSNLGCN with others RP-type air electrode previously reported.

Air electrode	Electrolyte thickness (μm)	Air electrode-feeding gas	Temperature (°C)	Current density (A cm^{-2}) at 1.3 V	Reference
$Pr_2NiO_{4+\delta}$-$BaZr_{0.2}Ce_{0.6}Y_{0.2}O_{3-\delta}$ (PNO-BZCY)	19	40% Air/ 60% H_2O	650 600	0.6 0.3	[10]
$Pr_{1.7}Ba_{0.3}NiO_{4+\delta}$ (PBN)	15	40% Air/ 60% H_2O	700 650 600	1.96 1.22 0.83	[11]
$La_{1.2}Sr_{0.8}NiO_4$ (LSN)	15	80% Air/ 20% H_2O	700 650 600	1.37 0.83 0.42	[7]
$Sr_{2.8}La_{0.2}Fe_2O_{7-\delta}$ (SLF)	20	80% Air/ 20% H_2O	700 600	1.08 0.46	[12]
$Nd_{1.9}Ba_{0.1}NiO_{4+\delta}F_{0.05}$ (NBNF)	25	50% Air/ 50% H_2O	700 650 600	1.37 0.75 0.36	[13]
$SrEu_2Fe_{1.8}Co_{0.2}O_{7-\delta}$ (SEFC)	15	90% Air/ 10% H_2O	700 650 600	1.4 0.7 0.4	[14]
$Pr_{0.4}Sr_{0.4}Nd_{0.4}La_{0.4}Gd_{0.4}Co_{0.5}Ni_{0.5}O_{4+\delta}$ (PSNLGCN)	**10**	**70% Air/ 30% H_2O**	**700 650 600**	**2.9 1.5 0.81**	**This work**

Reference

1 Z. F. Wang, X. Y. Miao, X. Z. Zhu, S. H. Guo, D. L. Han, X. F. Ye, Z. Y. Wen, *J. Power Sources,* 2024, ***597***, 234141.

2 Y. Y. Sun, J. Zhou, Z. R. Liu, Z. L. Zhou, J. M. Yang, H. F. Zhao, C. F. Yin, K. Wu, Y. Liu, *Int. J. Hydrogen Energy,* 2024, ***50***, 1622-1631.

3 Y. Q. Zhao, K. Zhang, Z. L. Wei, Z. B. Li, Y. Wang, Z. W. Zhu, T. Liu, *Electrochim. Acta,* 2020, ***352***, 136444.

4 A. Grimaud, F. Mauvy, J. M. Bassat, S. Fourcade, L. Rocheron, M. Marrony, J. C. Grenier, *J. Electrochem. Soc.,* 2012, ***159***, B683-B694.

5 H. G. Shi, C. Su, X. M. Xu, Y. L. Pan, G. M. Yang, R. Ran, Z. P. Shao, *Small,* 2021, ***17***, 2101872.

6 Z. Yang, J. Zhang, B. X. Wu, X. Zhao, X. L. Lu, Y. C. Zhao, Y. D. Li, *Ceram. Int.,* 2023, ***49***, 25381-25388.

7 S. J. Yang, Y. B. Wen, J. C. Zhang, Y. Lu, X. F. Ye, Z. Y. Wen, *Electrochim. Acta,* 2018, ***267***, 269-277.

8 J. Y. Ma, Y. X. Pan, Y. K. Wang, Y. Chen, *J. Power Sources,* 2021, ***509***, 230369.

9 Z. Z. Chen, J. L. Wang, D. M. Huan, S. J. Sun, G. P. Wang, Z. P. Fu, W. H. Zhang, X. S. Zheng, H. B. Pan, R. R. Peng, Y. L. Lu, *J. Power Sources,* 2017, ***371***, 41-47.

10 W. Y. Li, B. Guan, L. Ma, S. S. Hu, N. Zhang, X. B. Liu, *J Mater Chem A,* 2018, ***6***, 18057-18066.

11 W. Y. Li, B. Guan, T. Yang, Z. Q. Li, W. Y. Shi, H. C. Tian, L. Ma, T. L. Kalapos, X. B. Liu, *J. Power Sources,* 2021, ***495***, 229764.

12 D. M. Huan, W. H. Wang, Y. Xie, N. Shi, Y. H. Wan, C. R. Xia, R. R. Peng, Y. L. Lu, *J Mater Chem A,* 2018, ***6***, 18508-18517.

13 A. P. Tarutin, G. K. Vdovin, D. A. Medvedev, A. A. Yaremchenko, *Electrochim. Acta,* 2020, ***337***, 135808.

14 D. M. Huan, N. Shi, L. Zhang, W. Z. Tan, W. H. Wang, C. R. Xia, R. R. Peng, Y. L. Lu, *Acs Applied Materials & Interfaces,* 2018, ***10***, 1761-1770.